FINITE ELEMENTS AND VOLUMES IN A EULER-LAGRANGE FORMULATION - artificial dissipation versus limited flux schemes

R. Akkerman, J. Huétink & P.N. van der Helm

University of Twente, Department of Mechanical Engineering
P.O. Box 217, 7500 AE Enschede, The Netherlands.

ABSTRACT

The convective part of a time-stepping Euler-Lagrange finite element formulation can be formulated in various ways. In this paper a finite element interpolation is compared to a finite volume formulation. The first algorithm is based on an averaging procedure used in postprocessing of finite element calculations. The second algorithm describes the fluxes through the element sides and stems from a finite difference method for compressible fluid dynamics. Both approaches have complementary characteristics with respect to accuracy and implementation.

1. INTRODUCTION

In the simulation of forming processes large material deformations, history dependent material behaviour and contact phenomena play an important role. Lagrangian formulations are well suited for problems concerning path-dependent material properties and free surfaces but suffer from numerical problems when the mesh is distorted heavily. Eulerian formulations are able to cope with large material deformations but are less suited for the description of history dependent material and free surfaces in transient problems. In Euler-Lagrange formulations, commonly denoted as "Arbitrary" Lagrangian-Eulerian (ALE) formulations, the mesh and material deformations are uncoupled. These formulations can handle path-dependent material behaviour and free surfaces while keeping the mesh regular.

The method can handle typically transient processes, such as upsetting of a metal billet (Fig. 1) as well as stationary processes, such as polymer extrusion (Fig. 2). The first example has mainly Lagrangian characteristics but keeps the mesh regular, the second example has mainly Eulerian characteristics but follows the free surface movements.

A number of Euler-Lagrange formulations for the simulation of forming processes are reported in literature. The methods can be divided into two groups, respectively coupled and split formulations. In the first formulation the coupled

Euler-Lagrange equations are solved, see for instance the work of Liu et al [3].

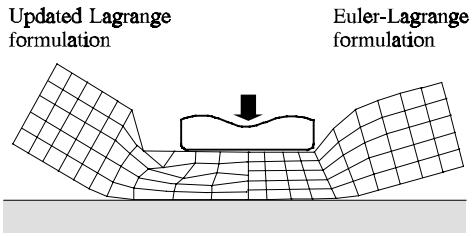

Fig. 1 Upsetting process.

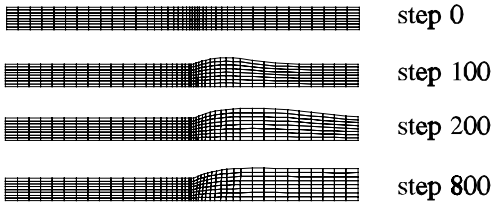

Fig. 2 Transient simulation of steady state polymer extrusion.

The tangent stiffness matrix consists of an ordinary Lagrangian and an additional Eulerian part. In the second approach the Euler-Lagrange equations are split and solved separately, see for example the work of Benson [4], Baaijens [5] and Huétink [1,6,7]. A normal Lagrangian step is performed, followed by an explicit (purely convective) Eulerian step. In this work the split Euler-Lagrange formulation is used.

In the next section two different Euler algorithms are described: an artificial dissipation and a limited flux scheme. In the subsequent section the implementation of the Euler formulations in the updated Lagrangian finite element code is addressed and three testcases are discussed. Finally, the conclusions are presented.

2. EULER FORMULATION

2.1. General remarks

A graphical interpretation of the Euler formulation is found by considering a mesh which is a result of a previous Lagrangian step and a neighbouring mesh where the simulation has to be continued. The integration point values (stress, strain, etc.) of the Lagrangian mesh have to be remapped to the new mesh, see figure 3.

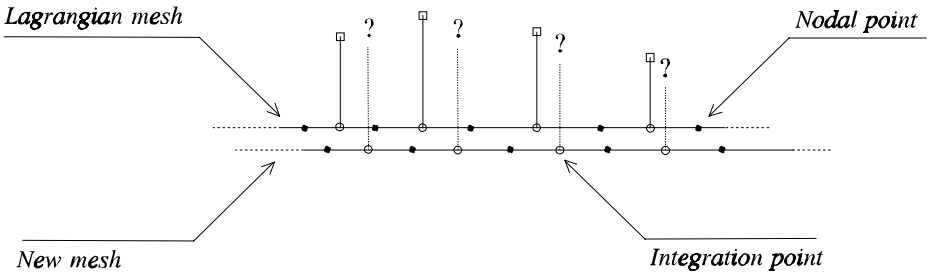

Fig. 3 Remapping integration point values.

The remapping is established by constructing a function based on the integration point data of the original Lagrangian mesh. This approximation is used to evaluate the integration point values of the new mesh.

A mathematical representation of the Euler step is given by the advection equation.

$$\frac{\partial f}{\partial t} + \boldsymbol{V} \cdot \frac{\partial f}{\partial \boldsymbol{x}} = 0 \qquad (1)$$

The advected quantity is denoted by *f*, the relative velocity between the material and mesh is given by ***V***. The remapping can be established by solving the advection problem. In literature various schemes can be found which deal with this problem.

The Euler formulation has to satisfy some requirements [4]. In the first place the approximation should be accurate: error analysis can be performed to determine the order of accuracy. Secondly, the estimation should be stable. This requirement is important when discontinuous functions, which frequently occur in the numerical simulation of plasticity, have to be remapped. Furthermore, the Euler step should be consistent: if the Lagrangian and Arbitrary mesh coincide the integration point values of both meshes should be the same. Subsequently, the remapping should be efficient since each independent variable has to be remapped in every iteration or increment.

2.2. One-dimensional grids

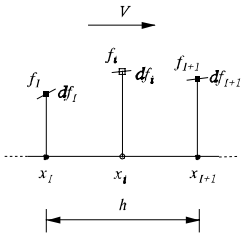

Fig. 4 1D staggered grid

The convective schemes will be illustrated using a regular, one-dimensional, staggered grid with one integration point and two nodes per element, see figure 4. Integration and nodal point values carry respectively lowercase and uppercase indices *i* and *I*. The values of the Lagrangian mesh at time *t* and the arbitrary mesh at time $t+\Delta t$ are respectively denoted by subscript and superscript indices. The relative velocity *V* is assumed to be positive for the time being. The extension of the following derivations to negative values of *V* is straightforward.

Both the finite element interpolation and the finite volume formulation are described as an adaptation of the Lax-Wendroff finite difference scheme:

$$f^i = f_i - C(f_i - f_{i-1}) - \tfrac{1}{2}C(1-C)(f_{i+1} - 2f_i + f_{i-1}) \qquad (2)$$

or, equivalently:

$$f^i = \tfrac{1}{4}(1+2C)f_{i-1} + \tfrac{1}{2}f_i + \tfrac{1}{4}(1-2C)f_{i+1} - \tfrac{1}{4}(1-2C^2)(f_{i+1} - 2f_i + f_{i-1}) \qquad (3)$$

where *C* is the Courant number $V\Delta t/h$ which is a measure for the relative displacement between the material and mesh.

The Lax-Wendroff scheme is second order accurate in space and time but exhibits spurious oscillations around discontinuities of the solution. To remedy these instabilities artificial dissipation can be added to the Lax-Wendroff scheme or the antidiffusive flux in the Lax-Wendroff scheme can be limited. Hence, one has to compromise between the accuracy and stability requir-ements. The Lax-Wendroff scheme is consistent since $C=0$ results in $f^i=f_i$.

Finite element interpolation scheme 1D

The starting point for the one-dimensional finite element scheme is equation (3). The term $2C^2$ is replaced by an artificial dissipation variable α:

The variable α results in artificial dissipation when $\alpha>2C^2$ and should vanish for zero Courant number *C* to satisfy the consistency requirement mentioned above. A

$$f^i = \tfrac{1}{4}(1+2C)f_{i-1} + \tfrac{1}{2}f_i + \tfrac{1}{4}(1-2C)f_{i+1} - \tfrac{1}{4}(1-\alpha)(f_{i+1} - 2f_i + f_{i-1}) \quad (4)$$

suitable function for the artificial dissipation variable is $\alpha=A|C|$ where A is an artificial dissipation parameter which is normally set to $A=1.5$.

The finite element form of equation (4) is given by:

$$f^i = \sum_{K=I}^{I+1} N_K(-C)f_K + (1-\alpha)(f_i - \sum_{K=I}^{I+1} N_K(0)f_K) \quad (5)$$

Thus, the new integration point value consists of the locally smoothed function as proposed by Hinton [8] (for postprocessing purposes) with an addition as proposed in [9]. Note that all the information necessary for the update of the integration point value is kept within the element.

Finite volume scheme 1D

For this one-dimensional limited flux scheme we start from equation (2). The antidiffusive flux is restricted by introducing a limiter function ϕ in the second order term:

$$f^i = f_i - C(f_i - f_{i-1}) + - \tfrac{1}{2}C(1-C)\left(\phi(r_{i+\frac{1}{2}})(f_{i+1} - f_i) - \phi(r_{i-\frac{1}{2}})(f_i - f_{i-1})\right) \quad (6)$$

The ratios of successive gradients are given by:

$$r_{i+\frac{1}{2}} = \frac{f_i - f_{i-1}}{f_{i+1} - f_i}, \quad r_{i-\frac{1}{2}} = \frac{f_{i-1} - f_{i-2}}{f_i - f_{i-1}} \quad (7)$$

The limiter function can be constructed using the concept of Total Variation Diminishing (TVD) schemes, resulting in a solution without wiggles. A number of limiter functions have been proposed, see for instance the work of Van Leer [9], Sweby [10] and Hirsch [11]. Here, the Van Leer limiter function is used:

$$\phi(r) = \frac{r + |r|}{1 + |r|} \quad (8)$$

Equation (6) can be expressed in terms of integration point values, averaged nodal values and gradients of the considered element:

$$f^i = f_i - 2C(f_i - f_I) + \\ -C(1-C)\left(\phi(r_{i+\frac{1}{2}})(f_{I+1} - f_i) - \phi(r_{i-\frac{1}{2}})(f_i - f_I)\right) \tag{9}$$

where the ratios of successive gradients are given by:

$$r_{i+\frac{1}{2}} = \frac{f_i - f_I}{f_{I+1} - f_i}, \quad r_{i-\frac{1}{2}} = \frac{f_I - f_i - df_i + 2df_I}{f_i - f_I} \tag{10}$$

with the element gradient and averaged nodal gradient repectively:

$$df_i = f_{I+1} - f_I, \quad df_I = \frac{1}{2}(df_{i-1} + df_i) \tag{11}$$

and the usual averaged nodal values.

Note that again all the data necessary for the calculation of the new integration point value are available within the element when also the gradients are stored at the nodal points and the integration points.

2.3. Two-dimensional grids

We now proceed to regular, two-dimensional, staggered grids with one integration point and four nodes per element. The relative velocity vector ***V*** is assumed to have positive components. The extension of the following to an arbitrary direction of ***V*** is straightforward. For the artificial dissipation and limited flux schemes, a different location of the averaged nodes is chosen, see figure 5.

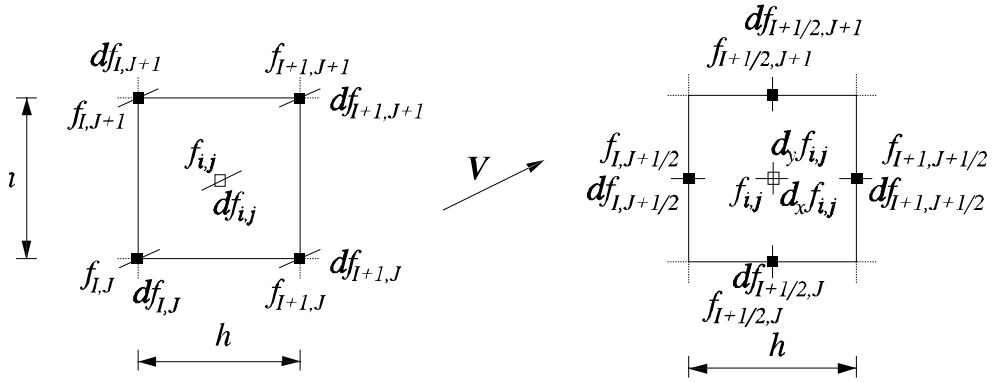

Fig. 5 2D grids for finite element (left) and finite volume scheme (right)

Finite element interpolation 2D

In multiple dimensions again the FE-discretization can be applied, giving the extension of equation (5):

with Courant numbers $C_x = V_x \Delta t / \mathrm{h}$ and $C_y = V_y \Delta t / \mathrm{h}$.

$$f^{i,j} = \sum_{K=I}^{K=I+1} \sum_{L=J}^{L=J+1} N_{K,L}(-C_x,-C_y) f_{K,L} + \\ + (1-\alpha)\left(f_{i,j} - \sum_{K=I}^{K=I+1} \sum_{L=J}^{L=J+1} N_{K,L}(0,0) f_{K,L} \right) \tag{12}$$

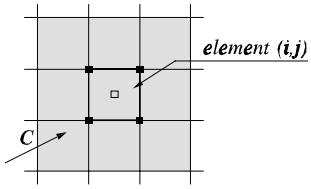

A graphical representation of the 2D artificial dissipation scheme (12) is given in figure 6. The shaded elements contribute indirectly by means of the averaged corner nodes to the update of the integration point value of element *(i,j)*.

Fig. 6 Corner coupling

The artificial dissipation variable for the 2D case is chosen $\alpha=A|\boldsymbol{C}|$ similar to the 1D situation: the one parameter artificial dissipation scheme. The discretization error introduced by equation (14) is [12]:

$$r^{i,j} = \tfrac{1}{4}h^2(\alpha-2C_x^2)\left(\frac{\partial^2 f}{\partial x^2}\right)_{i,j} + \tfrac{1}{4}h^2(\alpha-2C_y^2)\left(\frac{\partial^2 f}{\partial y^2}\right)_{i,j} + O(h^3) \tag{13}$$

The accuracy of the artificial dissipation scheme (12) depends on the flow direction. When $|C_x|=|C_y|$ and the one parameter artificial dissipation scheme is adapted to $\alpha=2C^2$ with $C=\max(|C_x|,|C_y|)$, both terms on the right hand side of equation (13) vanish, resulting in a second order accurate scheme. For flow in other than diagonal directions a term of order h^2 remains unequal to zero on the right hand side, leading to crosswind diffusion.

The function for the artificial dissipation variable can be refined by taking into account the curvature of the field f in the flow direction. Similar procedures have been reported in literature [13,14]. Suppose that a dimensionless measure for the curvature $\kappa\in[0,1]$ in element *(i,j)* is available: κ is small when the curvature is small and equal to one when the curvature is large. The artificial dissipation variable can then be chosen as $\alpha=\kappa A|\boldsymbol{C}|$: the two parameter artificial dissipation scheme. A possible measure for the curvature is given by:

$$\kappa = \begin{cases} K, & K \le 1 \\ 1, & K > 1 \end{cases}$$
$$K = B\frac{|d_0|}{\min(|d_1|,|d_2|)} \tag{14}$$

The nominator and denominator parameters are:

$$
\begin{aligned}
d_0 &= \sum_{K=I}^{K=I+1}\sum_{L=J}^{L=J+1} \frac{N_{K,L}(-C_x,-C_y) - N_{K,L}(0,0)}{|\boldsymbol{C}|}\, df_{K,L} \approx h^2 \left(\frac{\partial^2 f}{\partial n^2}\right)_{i,j} \\
d_1 &= \sum_{K=I}^{K=I+1}\sum_{L=J}^{L=J+1} \frac{N_{K,L}(-C_x,-C_y) - N_{K,L}(0,0)}{|\boldsymbol{C}|}\, f_{K,L} \approx h \left(\frac{\partial f}{\partial n}\right)_{i,j} \\
d_2 &= f_{i,j}
\end{aligned}
\qquad (15)
$$

where $\boldsymbol{n}=\boldsymbol{V}/|\boldsymbol{V}|$ is the unit vector in flow direction and the first denominator term d_1 is equal to the element gradient $df_{i,j}$. The derivative with respect to $\boldsymbol{n}$ represents the component of the gradient in the flow direction: $\partial f/\partial \boldsymbol{n} = \nabla f \cdot \boldsymbol{n}$. The gradients in the nodal points are determined with the usual averaging procedure

Appropriate values for the dissipation parameters *A* and *B* depend to a certain degree on the type of problem and can be found by performing numerical experiments on suitable testcases, see the next section. A proper choice for the parameter *A* appears to be *A=1.5*. The choice for *B* depends on the curvature of the field. For small curvatures *B=0.05* is sufficient, for larger curvatures *B=0.5* will do the job. Note that for large values of *B* the two parameter model reduces to the one parameter model since in that case κ equals unity.

Finite volume scheme 2D

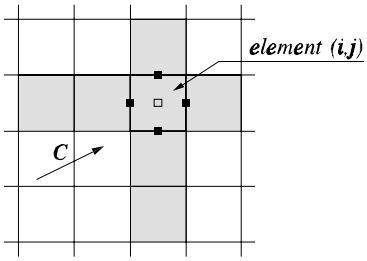

Fig. 7 Side coupling of the 2D limited flux scheme

The multi-dimensional finite volume scheme is found by addition of the fluxes through the element sides in both coordinate directions. This is a straightforward generalization of equation (9).

The scheme is represented in figure 7. The shaded elements add indirectly via the the averaged mid-side nodes to the update of the integration point values of element *(i,j)*. Note the side coupling of this element to the adjacent elements.

The accuracy of the limited flux scheme varies with the flow direction. When assuming that $|C_x| \gg |C_y|$, the scheme reduces to a set of 1D limited flux schemes (9) with nearly second order accuracy. The accuracy decreases when material is advected between elements that have only one corner node in common, for example when $|C_x| = |C_y|$.

When comparing the different Euler formulations it is clear that the one parameter artificial dissipation scheme is the most simple scheme and the cheapest with respect to the number of operations and data storage per element. The two parameter artificial dissipation scheme and the limited flux scheme are more complicated and require more data manipulation and storage.

At the end of each timestep the averaged nodal values are determined. In the next step these nodal values can be elaborated to element gradients, which in turn can be elaborated to nodal averaged gradients. It will be clear that these nodal averaged gradients lag one extra step behind. For the artificial dissipation scheme

this appears to give no problems, since the nodal gradients have only an indirect influence through the curvature parameter. For the limited flux scheme, however, the gradients have a direct influence on the accuracy and have to be updated in an extra loop at the end of each timestep.

3. EULER-LAGRANGE FORMULATION

The Euler-Lagrange formulation is a combination of the Euler and the updated Lagrange formulation. The requirements of the Euler formulation are listed in the preceding section. The requirements of the Lagrange formulation are dictated by the balance of mass and momentum and the constitutive equations. Hence, no material should be added or lost in the bulk or at the boundaries. Furthermore, the introduced mechanical unbalance should be sufficiently small, otherwise the incremental-iterative solution procedure will diverge. Subsequently, the Cauchy stress tensor and equivalent plastic strain should be compatible and the equivalent plastic strain should remain non-negative.

Basically two different Euler-Lagrange formulations are possible when a split algorithm has been chosen. In the first approach the Euler algorithm is applied after the iteration loop of an updated Lagrange step. In the second strategy the Euler algorithm is embedded in the iteration loop. The advantage of the first method over the second one is that the Euler algorithm is applied once per time step. The disadvantage is the lack of checking of the mechanical equilibrium after applying the Euler algorithm.

In the current Euler-Lagrange formulation the second approach is adopted. In every iteration an updated Lagrange predictor step is followed by a Euler algorithm, determining the upstream conditions, and an updated Lagrange evaluation of the material increments of stress, strains etc.

Linear quadrilateral, constant dilatation elements for plane strain and axisymmetric analysis have been used here. The artificial dissipation scheme is evaluated at the four integration point locations, the limited flux scheme at the element center. The midpoint values are found by averaging the four integration point values. The Courant vector $\boldsymbol{C}$ is equal to the isoparametric representation of the convective displacement.

4. APPLICATIONS

The behaviour of the two convective schemes in different flow directions is illustrated by a pure advection problem on a course grid.

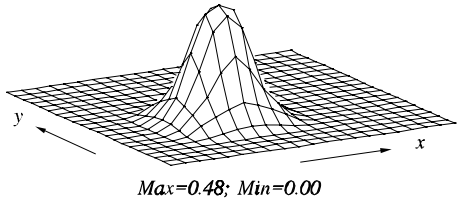

Consider a patch of *20×20 mm* rigid-ideally plastic material. The patch is modelled using *20×20* constant dilatation plane strain elements. The patch is prestrained, the initial plastic strain distribution is shown in figure 8.

Fig. 8 Initial plastic strain distribution.

The plastic strain pulse is advected by translating the mesh in the (ΔU,ΔV) direction and remapping the integration point values to the initial mesh. Two advection cases are considered: in the first case the displacement increments are $\Delta U=0.5$ *mm* and $\Delta V=0.0$ *mm* (advection parallel to mesh), in the second case $\Delta U=0.5$ *mm* and $\Delta V=0.5$ *mm* (advection diagonal to mesh). The total number of increments is *10*. Two Euler formulations are used: an adaptation of the one parameter artificial dissipation scheme with $\alpha=2C^2$ where $C=\max(|C_x|,|C_y|)$ and the limited flux scheme. The results of the artificial dissipation and limited flux schemes for parallel and diagonal advection are shown below.

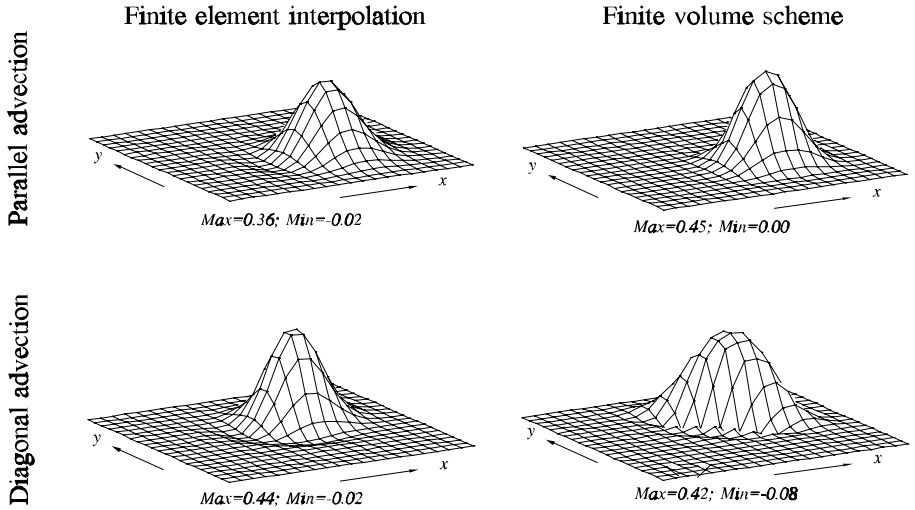

Fig. 9 Resulting plastic strain distributions.

It is clear that the accuracy of the Euler formulation depends on the flow direction. For this particular testcase the limited flux scheme gives the best results when the advection is parallel to the mesh, the artificial dissipation scheme gives the best outcome when the advection is diagonal to the mesh. These results agree well with the discussion on the accuracy of the artificial dissipation and limited flux schemes in section 2. Note that the limited flux scheme is monotone when the advection is parallel to the mesh.

An application of the method is a wire drawing problem, with interaction between the Cauchy stress tensor and the plastic strain. When the constraining forces of the die are removed in the outlet zone, the elastoplastic behaviour of the material will lead to a redistribution of the internal stresses. All plots are based on corner node averaged values.

Consider a wire drawn from the right to the left through a die. One half of the wire is modelled using *6x31* constant dilatation axisymmetric elements. The elastic material behaviour of the wire is defined by the Young's modulus *E=200,000 N/mm*^{2} and Poisson's

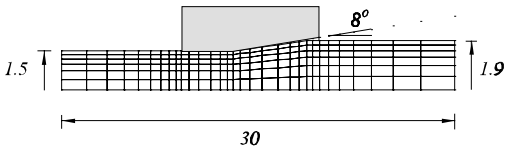

Fig. 10 Wire drawing mesh.

ratio $\nu=0.3$. The initial yield stress is $\sigma_{y0}=250\ N/mm^2$. The plastic material behaviour is represented by a Von Mises model. Hardening is described according to the relation between the equivalent plastic strain ε_p and yield stress σ_y is given by a Voce equation:

$$\sigma_y = \sigma_{y0} + D\left(1 - e^{-\frac{\varepsilon_p}{\varepsilon_{p0}}}\right) \tag{25}$$

where $D=200\ N/mm^2$ and $\varepsilon_{p0}=0.3$.

The wire is drawn in *320* increments to the total displacement *U=15 mm*. The solution is continuously remapped to the initial mesh. The resulting solution is stationary. Three Euler-Lagrange simulations are carried out using respectively the one parameter artificial dissipation scheme with *A=1.5*, the two parameter artificial dissipation scheme with *A=1.5*, *B=0.05* and the limited flux scheme. The resulting plastic strains and axial stresses are depicted below.

From these figures is clear that all formulations give acceptable results. Differences between the three schemes are observed in the outlet zone left from the die. In that region the isolines of the equivalent plastic strain diverge for the one parameter artificial dissipation model due to crosswind diffusion.

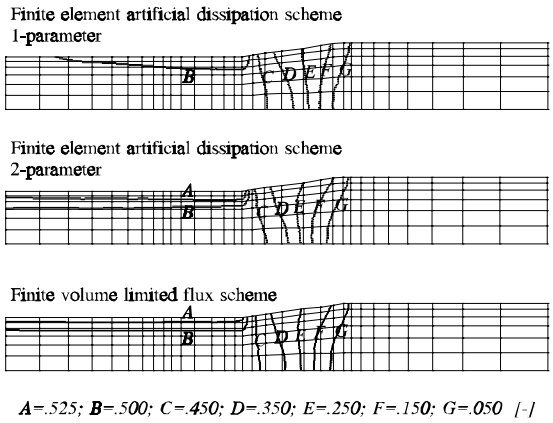

Fig. 11 Resulting plastic strain distributions

For the two parameter model some small wiggles in the isolines are noticed. The limited flux scheme displays nearly no crosswind diffusion in the outlet zone and is stable.

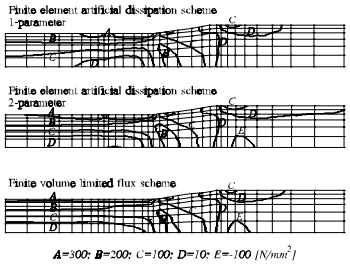

Fig. 12 Resulting axial stress distributions.

5. CONCLUSIONS

In this paper two split Euler-Lagrange formulations are discussed. The Euler step of the first Euler-Lagrange formulation is based on an artificial dissipation scheme, the second on a limited flux scheme. For the one-dimensional case it can be shown that both schemes are basically a Lax-Wendroff finite difference scheme. For the two-dimensional case they differ considerably. The implementation of both methods is different: the artificial dissipation scheme uses averaged corner nodes, the limited flux scheme uses averaged mid-side nodes. Furthermore, the accuracy of both schemes is different: the artificial dissipation scheme is more accurate when the relative displacements are skew to the mesh, the limited flux scheme is

more precise when the relative displacements are parallel to the mesh. We can conclude that both schemes have complementary virtues.

However, when the Euler-Lagrange simulation has mainly Lagrangian characteristics, which is the case for the upsetting process mentioned in the introduction, the accuracy of the Euler algorithm is of minor importance. When the Euler-Lagrange simulation has mainly Eulerian characteristics, which is the case for the extrusion and wire drawing process mentioned before, the accuracy of the Euler algorithm is of more importance.

ACKNOWLEDGEMENTS

The authors thank Jan-Willem van der Burg for his comments on the limited flux schemes.

REFERENCES

1. HUÉTINK, J., VREEDE, P.T. and VAN DER LUGT, J. Progress in mixed Eulerian-Lagrangian finite element simulation of forming processes, *Int. J. Num. Meth. Eng.*, 30, 1441-1457, 1990.
2. AKKERMAN, R., *Euler-Lagrange simulations of nonisothermal viscoelastic flows* (thesis), University of Twente, Enschede, 1993.
3. LIU, W.K., CHANG, H., CHEN J.S. and BELYTSCHKO, T. Arbitrary Lagrangian-Eulerian Petrov-Galerkin finite elements for nonlinear continua, *Comp. Meth. Appl. Mech. Eng.*, 68, 259-310, 1988.
4. BENSON, D.J., An efficient, accurate, simple ALE method for nonlinear finite element programs, *Comp. Meth. Appl. Mech. Eng.*, 72, 305-350, 1989.
5. BAAIJENS, F.P.T., An U-ALE formulation of 3-D unsteady viscoelastic flow, *Int. J. Num. Meth. Eng.*, 36, 1115-1143, 1993.
6. HUÉTINK, J., *On the simulation of thermo-mechanical forming processes - A mixed Eulerian-Lagrangian finite element method* (thesis), University of Twente, Enschede, 1986.
7. HUÉTINK, J. and HELM, P.N. VAN DER. On Euler-Lagrange finite element formulation in forming and fluid problems, *Proc. 4th Int. Conf. NUMIFORM*, 1992.
8. HINTON, E. and CAMPBELL, J.S. Local and global smoothing of discontinuous finite element functions using a least squares method, *Int. J. Num. Meth. Eng.*, 8, 461-480, 1974.
9. LEER, B. VAN. Towards the ultimate conservative difference scheme. V. A second-order sequel to Godunov's method, *J. Comp. Phys.*, 32, 101-136, 1979.
10. SWEBY, P.K. High resolution schemes using flux limiters for hyperbolic conservation laws, *Siam J. Num. Anal.*, 21, 995-1010, 1984.
11. HIRSCH, C. *Numerical computation of internal and external flows 2*, John Wiley & Sons, New York, 1988.
12. HELM, P.N. VAN DER. Investigation and implementation of an ALE algorithm, *TNO report* BI-92-112, 1992.
13. BROOKS, A.N. and HUGHES, T.J.R. Streamline upwind/Petrov-Galerkin formulations for convection dominated flows with particular emphasis on the incompressible Navier-Stokes equations, *Comp. Meth. Appl. Mech. Eng.*, 32, 199-259, 1982.
14. DONEA, J. Arbitrary Lagrangian-Eulerian finite element methods, In: T. Belytchko and T.J.R. Hughes, editors, *Comp. Meth. in Mech. 1*, Elsevier Science Publishers B.V., Amsterdam, 1983.